Atmos. Chem. Phys. Discuss., 15, 10085–10122, 2015
www.atmos-chem-phys-discuss.net/15/10085/2015/
doi:10.5194/acpd-15-10085-2015

Atmospheric Chemistry and Physics
Discussions
Open Access

A method for merging nadir-sounding climate records, with an application to the global-mean stratospheric temperature data sets from SSU and AMSU

C. McLandress[1], T. G. Shepherd[2], A. I. Jonsson[1], T. von Clarmann[3], and B. Funke[4]

[1]Department of Physics, University of Toronto, Toronto, Canada
[2]Department of Meteorology, University of Reading, Reading, UK
[3]Karlsruhe Institute of Technology, Karlsruhe, Germany
[4]Instituto de Astrofísica de Andalucía, Granada, Spain

Received: 8 January 2015 – Accepted: 13 March 2015 – Published: 2 April 2015

Correspondence to: C. McLandress (charles@atmosp.physics.utoronto.ca)

Published by Copernicus Publications on behalf of the European Geosciences Union.

Abstract

A method is proposed for merging different nadir-sounding climate data records using measurements from high resolution limb sounders to provide a transfer function between the different nadir measurements. The nadir-sounding records need not be overlapping so long as the limb-sounding record bridges between them. The method is applied to global mean stratospheric temperatures from the NOAA Climate Data Records based on the Stratospheric Sounding Unit (SSU) and the Advanced Microwave Sounding Unit-A (AMSU), extending the SSU record forward in time to yield a continuous data set from 1979 to present. SSU and AMSU are bridged using temperature measurements from the Michelson Interferometer for Passive Atmospheric Sounding (MIPAS), which is of high enough vertical resolution to accurately represent the weighting functions of both SSU and AMSU. For this application, a purely statistical approach is not viable since the different nadir channels are not sufficiently linearly independent, statistically speaking. The extended SSU global-mean data set is in good agreement with temperatures from the Microwave Limb Sounder (MLS) on the Aura satellite, with both exhibiting a cooling trend of $\sim 0.6 \pm 0.3\,\mathrm{K\,decade^{-1}}$ in the upper stratosphere from 2004–2012. The extended SSU data set also compares well with chemistry-climate model simulations over its entire record, including the contrast between the weak cooling seen over 1995–2004 compared with the large cooling seen in the period 1986–1995 of strong ozone depletion.

1 Introduction

Stratospheric cooling has long been regarded as a key indicator of two anthropogenic climate forcings (IPCC 2013; WMO 2014): that from increasing abundances of CO_2, and that from the ozone decline associated with the increased abundances of ozone-depleting substances (ODSs). The former has continued secularly, while the latter peaked in the late 1990s and has been slowly declining since then. Thus, the con-

ACPD
15, 10085–10122, 2015

trast between the early and more recent parts of the stratospheric temperature record is an important fingerprint of anthropogenic influence (Shepherd and Jonsson, 2008). In addition to the anthropogenic influences, stratospheric temperature is also strongly perturbed by the 11 year solar cycle and by volcanic eruptions. As a consequence, the anthropogenic cooling is considerably modulated in time.

In the stratosphere, global mean temperature is, to a first approximation, unaffected by dynamics and is therefore close to radiative equilibrium (Fomichev, 2009). This makes it an ideal quantity for detection and attribution of anthropogenic influence (Shine et al., 2003). However, global averages are only obtainable from satellites, and the only long-term satellite record of stratospheric temperature is that from the operational nadir sounders, the Stratospheric Sounding Unit (SSU)/Microwave Sounding Unit (MSU) and the Advanced Microwave Sounding Unit-A (henceforth AMSU) (Randel et al., 2009), which represent deep atmospheric layers. Note that the vertically resolved temperature data from Global Positioning System (GPS) radio occultation only begin in the current century, and do not reach into the upper stratosphere, where the strongest cooling is found. The nadir sounding measurements were never designed for climate monitoring, and homogenizing the data from different operational satellites, with rapidly drifting orbits, is a challenge (Wang et al., 2012; Zou et al., 2014).

In the lower stratosphere, the relevant nadir record is provided by MSU Channel 4 (and continued by AMSU) and is supplemented by radiosondes and, since the early 2000s, by GPS radio occultation. The global-mean MSU4 record is considered fairly reliable and most attention has focused on its latitudinal structure (Randel et al., 2009).

The middle and upper stratosphere is, however, a completely different story. There the nadir record is provided by three SSU channels which began in 1979 and ended in 2006, and by six AMSU channels which began in 2001 and are ongoing. Because the weighting functions of the SSU and AMSU channels are very different, the two records cannot be immediately combined. Moreover, confidence in the SSU record has been low, even for global-mean temperature, because of the lack of corroborative measurements, drift issues within the SSU record itself, and the striking differences

ACPD
15, 10085–10122, 2015

identified by Thompson et al. (2012) between the two SSU products available at that time (from the National Oceanic and Atmospheric Administration (NOAA) and the Met Office) and between the measurements and chemistry-climate models.

Normally, differences between measurements and models would tend to cast suspicion on the models, not the measurements. However, because global-mean stratospheric temperature is radiatively controlled, its behaviour in the middle and upper stratosphere, where the radiative processes are well understood, should be reasonably well represented by chemistry-climate models. Indeed, Fig. 2 of Thompson et al. (2012) shows that for the SSU channels the differences in cooling between models and observations, and between the Met Office and NOAA products of the time, are in almost all cases much larger than the inter-model spread. One of the mysteries arising from Thompson et al. (2012) was the apparent lack of continued cooling in the SSU record during the early 2000s, in contrast to the models and in contradiction to physical expectations. Because the SSU record ended in 2005, this mystery was unresolved.

In this paper, we propose a method for merging different nadir-sounding climate data records, and apply it to the NOAA SSU and AMSU global-mean stratospheric temperature records. Specifically we use the AMSU data to extend the three SSU channels forward in time, given the paradigmatic importance of that climate data record. We show that a purely statistical approach, using multiple linear regression, is unworkable for this particular application since the six AMSU channels are not sufficiently linearly independent. Instead, we propose a physically based method using limb-sounding measurements, with much higher vertical resolution, to accurately represent the weighting functions of both SSU and AMSU, and thereby act as a transfer function between the two nadir-sounding data sets. For this purpose we use temperature data from the Michelson Interferometer for Passive Atmospheric Sounding (MIPAS).

Since we are dealing with monthly-mean, global-mean data, the data are highly averaged and the effect of random measurement errors is expected to be low. Characterization of the systematic errors in such highly averaged quantities in a bottom-up fashion would be extremely challenging (Hegglin et al., 2013). Instead, our approach is to compare the different data sets (after transformation via the weighting functions) over their overlap periods to see whether the differences between them can be characterized in terms of a constant offset (within some noise). If this is the case, then the merging can be done with confidence. Thus, the validity of the approach can be assessed a posteriori. This approach was followed by Hegglin et al. (2014) in constructing a merged stratospheric water vapour record. Solomon et al. (2010) also performed such an additive relative bias correction to merge the HALOE and MLS stratospheric water vapour records. Thus there is ample precedent for such an approach in the literature.

The data sets used are described in Sect. 2. The merging methodology and the comparison between MIPAS and the two nadir sounding records are provided in Sect. 3.1. This comparison shows that the different global-mean data sets track each other very well, so additive relative biases can be identified with small uncertainties. Section 3.2 examines the (near) global-mean temperature trends, both over the recent record (as represented by the six AMSU channels) where we compare the MIPAS and AMSU trends to those from the Microwave Limb Sounder (MLS) on the Aura satellite, and over the extended SSU record. The extended SSU record is found to be in agreement with chemistry-climate models over the 1979–2011 period, including the continued cooling over the first decade of the 21st century. Conclusions are drawn in Sect. 4.

2 Description of data sets

2.1 SSU

We use version 2.0 brightness temperatures from SSU, as well as the corresponding weighting functions for the three channels. The data set is produced by the NOAA Center for Satellite Applications and Research (STAR) and is available at ftp://ftp.star.nesdis.noaa.gov/pub/smcd/emb/mscat/data/SSU/SSU_v2.0/.

The SSU data extend from 1979 to early 2006. See Zou et al. (2014) for a detailed discussion of the NOAA Version 2 SSU temperatures.

ACPD
15, 10085–10122, 2015

2.2 AMSU

We use brightness temperatures from AMSU, also analyzed by NOAA STAR (Wang and Zou, 2014), which are available at ftp://ftp.star.nesdis.noaa.gov/pub/smcd/emb/mscat/data/AMSU_v1.0/monthly. The corresponding weighting functions for channels 9 to 14 were provided courtesy of Likun Wang of NOAA STAR. The temperature data for Channels 9 to 13 start in January 1999; those for Channel 14 start two years later.

2.3 MIPAS

MIPAS is a limb sounder which measured infrared emission from which temperature and atmospheric constituents are derived (Fischer et al., 2008). We use zonal and monthly mean gridded temperatures computed from versions V3o_T_10 and V5r_T220 for the periods 2002–2004 and 2005–2011, respectively. These data are available at http://www.esa-spin.org/index.php/spin-data-sets and are provided on a 5° latitude grid with 28 pressure levels ranging from 300 to 0.1 hPa. The parent data were produced by the Institute for Meteorology and Climate Research at Karlsruhe Institute of Technology, in cooperation with the Institute of Astrophysics of Andalusia, from calibrated radiance spectra provided by the European Space Agency. The MIPAS temperature retrieval method is discussed in von Clarmann et al. (2003) for the high spectral resolution measurement period until 2004 and in von Clarmann et al. (2009) for the reduced spectral resolution measurement period from 2005 onwards. MIPAS temperatures have been validated by Wang et al. (2005) and Stiller et al. (2012).

2.4 MLS

Aura MLS has provided a nearly continuous set of measurements of temperature and trace gases in the middle atmosphere since August 2004. Here we use version 3.3

ACPD
15, 10085–10122, 2015

temperature data (Livesey et al., 2011) through the end of 2011. The temperature retrieval method and validation are discussed in Schwartz et al. (2008).

2.5 CMAM30

The CMAM30 data set, which extends from 1979 to 2011, is produced using a specified-dynamics version of the Canadian Middle Atmosphere Model (CMAM) that is driven by winds and temperatures from ERA Interim, where the global mean temperatures have been adjusted in the upper stratosphere to remove temporal discontinuities in 1985 and 1998 that have arisen from the introduction of new satellite data in the assimilation process (McLandress et al., 2014). Here we use the monthly mean CMAM30 temperatures, which are available at http://www.cccma.ec.gc.ca/data/cmam/output/CMAM/CMAM30-SD/mon/atmos/.

2.6 CCMVal2

Chemistry-climate model (CCM) simulations of the recent past from phase 2 of the CCM Validation project (CCMVal2) are used. These REF-B1 simulations use observed sea-surface temperatures and sea-ice distributions and observed forcings (volcanic aerosols, tropospheric concentrations of greenhouse gases, ozone-depleting substances, and solar variations). The model data are available at the SPARC Data Center at http://www.sparc-climate.org/data-center/data-access/. Although 16 models participated in CCMVal2, we use data from only the following 11 models: AMTRAC3, CCSRNIES, CMAM, EMAC-FUB, LMDZrepro, MRI, SOCOL, ULAQ, UMUKCA-METO, UMUKCA-UCAM and WACCM, where the model acronyms are defined in Morgenstern et al. (2010). The remaining five models were excluded either because they did not have a sufficiently high upper boundary, contained negative temperatures in the lower troposphere (perhaps due to extrapolation over Antarctica) or were outliers. The CCMVal2 models are described in Morgenstern et al. (2010).

ACPD
15, 10085–10122, 2015

2.7 ERA Interim

The interim version of the European Centre for Medium-Range Weather Forecasts Reanalysis (ERA Interim; Dee et al., 2011) temperature data set we use extends from 1979 to 2011. We also use the adjusted ERA-Interim global-mean temperatures that are used in CMAM30 (see Sect. 2.5), which are available at http://www.cccma.ec.gc.ca/data/cmam/cmam30/.

3 Results

The results section is divided into two parts. The first part (Sect. 3.1) pertains to the merging of the SSU and AMSU data sets. Since this is achieved using MIPAS data as a transfer function, we begin by demonstrating that MIPAS is in good agreement with SSU and AMSU. We then describe the algorithm used to merge SSU and AMSU, and present the merged results. The second part (Sect. 3.2) is an analysis of temperature trends for the post-2000 time period when the AMSU, MIPAS and MLS data are all available, as well as a comparison of our "extended" SSU results to other long term data sets, including models. All results presented here are for monthly and near-global means (75° S–75° N).

3.1 Merging SSU and AMSU

3.1.1 Comparisons to MIPAS

In order to compare MIPAS to SSU and AMSU, the MIPAS temperatures must be averaged in the vertical using the SSU and AMSU weighting functions, which are shown in the left and right panels of Fig. 1, respectively (thick solid curves). For simplicity we follow Thompson et al. (2012) in using fixed weighting functions, rather than attempting to account for possible state-dependence. The three SSU weighting functions (Channels 1–3) peak at approximately ~ 30, 39 and 44 km. The six stratospheric AMSU weighting functions (Channels 9–14) peak at ∼ 17, 20, 25, 30, 37 and 42 km. The other curves in the left panel of Fig. 1 will be discussed in due course.

The vertical averaging is performed on a log-pressure height grid, with the limits of integration being the corresponding height range of the MIPAS data: 300 hPa (∼ 8.4 km) and 0.1 hPa (∼ 64.5 km). The vertically averaged temperature for channel n (denoted T_n) is therefore given by

$$T_n(t) = \int_{z_b}^{z_t} T(t,z) W_n(z) \mathrm{d}z \quad (1)$$

where t is time in month and z is the log-pressure height [$z = -H \ln(p/p_s)$, with $H = 7$ km and $p_s = 1000$ hPa], and z_b and z_t are the limits of integration, namely z(300 hPa) and z(0.1 hPa). Before computing the vertical average, the weighting functions are normalized so that their vertical integral from z_b to z_t equals 1.

By excluding the lower troposphere and upper mesosphere in Eq. (1), the full vertical integrals of the weighting functions are approximated. This approximation is less accurate for SSU than it is for AMSU since the SSU weighting functions extend down lower and up higher than for AMSU (Fig. 1). To investigate the possible impact of this incomplete vertical averaging using the SSU weighting functions, we first filled the MIPAS temperature data below 300 hPa and above 0.1 hPa using the corresponding CMAM30 data, and then performed the integration using $z_b = 0$ km to $z_t \cong 100$ km. The resulting vertically averaged temperatures for the three SSU channels (not shown) are virtually indistinguishable from those obtained by averaging only over the MIPAS domain (8–65 km), leading us to conclude that the effect of the incomplete vertical sampling of the integral given by Eq. (1) is negligible.

Figure 2 compares the SSU-weighted MIPAS temperatures to SSU for 2002–2007, the years when the two instruments overlap. The thick and thin lines denote, respectively, the results with and without the seasonal cycle included, where the seasonal cycle is given by the first three harmonics of the annual cycle. The MIPAS time series have each been offset by a constant amount with respect to SSU, with the offset being determined so that the mean difference between the deseasonalized MIPAS and SSU time series is zero over the overlap period. The offsets are small: ~ -0.2 K for Channels 1 and 3 and ~ -0.7 for Channel 2. Although the overlap period between MIPAS and SSU is fairly short (4 years), and has several gaps, the agreement between the two is quite good.

Figure 3 shows the corresponding results for AMSU and AMSU-weighted MIPAS. As in Fig. 2, the MIPAS results are offset with respect to AMSU, with the magnitude of the offsets again all being less than 1 K. As seen with SSU, there is overall good agreement between MIPAS and AMSU, but with MIPAS exhibiting stronger cooling in the upper three channels (12–14). We will discuss this trend difference in Sect. 3.2 when we compare the trends to MLS.

3.1.2 Algorithm for merging SSU and AMSU

Having shown that the vertically weighted MIPAS temperatures are in good agreement with SSU and AMSU (apart from additive relative biases), we now proceed to merge the latter two data sets. Since the SSU and AMSU weighting functions differ in shape and height of the maxima, the two data sets must be combined by taking suitably weighted averages of the different channel temperatures. One way this might be done would be purely statistically, fitting the deseasonalized temperatures of instrument A to instrument B using multiple linear regression as follows

$$\hat{T}_n^{\mathrm{A}}(t) = \sum_{m=m_1}^{m_2} \alpha_m T_m^{\mathrm{B}}(t) \qquad (2)$$

where $\hat{T}_n^{\mathrm{A}}$ (with the hat) denotes the fitted deseasonalized temperature from Channel n of instrument A, T_m^{B} denotes the actual deseasonalized temperature from Channel m of instrument B, and the constants α_m are the coefficients determined using a least squares fit. However, this method, which we shall refer to as the temperature-fit method,

ACPD
15, 10085–10122, 2015

is problematic because the time series used in computing the fit (T_m^B) are highly linearly dependent, as is shown in Fig. 4 in the case where B = AMSU. The top panel shows the deseasonalized temperature anomalies for the six channels superimposed. Adjacent or near-adjacent channels are highly correlated. Given the overlap in the AMSU weighting functions (W), some correlation is to be expected. For example, for the highest three channels the overlap between W_{13} and W_{14} is ∼ 61 %, between W_{12} and W_{13} is ∼ 60 % and between W_{12} and W_{14} is ∼ 31 %. However, the fact that the correlations are actually close to unity for those pairs of channels, i.e., $r(13,14) \sim 0.96$, $r(12,13) \sim 0.96$ and $r(12,14) \sim 0.88$, suggests that they also reflect strong vertical relationships in the variability of global-mean temperature. A similarly high correlation of 0.91 is found between Channels 9 and 10, while Channel 11 is highly correlated with both Channel 10 ($r \sim 0.90$) and Channel 12 ($r \sim 0.87$). Thus, there appear to be only about two degrees of freedom among the six channels, representing the upper stratosphere and the lower stratosphere. Similarly high correlations are found, albeit with more noise, in the CMAM30 data shown in the bottom panel of Fig. 4, which is plotted over the 1979 to 2011 period. The high correlations between the different channel temperatures means that the system of equations defined by Eq. (2) is highly underconstrained, and that there are no unique values of the coefficients α_m. This was verified in a calculation in which one of the α_m's was specified and the remaining ones were computed, which yielded an almost identical temperature time series yet with very different coefficients. For this reason the temperature-fit method will not be used.

An alternative method, which is the method we have adopted, is to determine the fit coefficients from the weighting functions. Such a method has also been examined by the Remote Sensing Systems group, which has processed and combined the SSU data (C. Mears, personal communication, 2014). Using the weighting functions to generate the temperature fit coefficients makes physical sense since it is the channels of instrument B that have weighting functions peaking closer to the peak of a given weighting function of instrument A that should be given the most weight in the fit. Another advan-

ACPD
15, 10085–10122, 2015

tage of this method is that it does not require the two temperature data sets to overlap in time, as does the temperature-fit method.

The weighting function fit method proceeds as follows. We first express the channel-n weighting function of instrument A as a linear combination of the weighting functions of instrument B:

$$\hat{W}_n^{\mathrm{A}}(z) = \sum_{m=m_1}^{m_2} \beta_m W_m^{\mathrm{B}}(z) \tag{3}$$

where the hat denotes the fitted weighting function. The constants β_m are computed using least squares and are normalized so that $\sum_{m=m_1}^{m_2} \beta_m = 1$. The deseasonalized temperatures for Channel n of instrument A are then constructed as follows

$$\hat{T}_n^{\mathrm{A}}(t) = c_n + \sum_{m=m_1}^{m_2} \beta_m T_m^{\mathrm{B}}(t) \tag{4}$$

where the constants c_n represent an additive relative bias between the two measurements.

The dotted curves in the left panel of Fig. 1 are the fits to the three SSU weighting functions using the six AMSU weighting functions ($m_1 = 9$ and $m_2 = 14$), computed using Eq. (3), but before the β_m's are normalized. The values of the *unnormalized* β_m's are given in Table 1. The reason that they do not sum to unity is due to incomplete sampling of the target weighting function. As seen in Fig. 1 the fits to SSU Channels 1 and 2 are excellent, with the only significant departures from the true weighting function occurring below ~ 10 km and above ~ 50 km where the SSU weighting functions do not have much strength anyways. Not surprisingly, the fit is poorest for the upper SSU Channel 3 since there are no AMSU weighting functions that peak above it. The corresponding fits using the normalized β_m's are given by the thin solid curves.

The reason for normalizing the β_m's becomes apparent by considering the case of a constant temperature T_{o} profile with an assumption of no relative bias between

ACPD
15, 10085–10122, 2015

instruments A and B, in which case it can be easily shown that

$$c_n = T_o \left(1 - \sum_{m=m_1}^{m_2} \beta_m \right). \tag{5}$$

Since we have assumed no relative bias between the two instruments, c_n should vanish. This will only occur if $\sum_{m=m_1}^{m_2} \beta_m = 1$.

To compute c_n we use temperatures from a third instrument (C), which overlaps in time with instruments A and B and is of high enough vertical resolution that a sufficiently accurate representation of the temperatures obtained from the weighting functions of both instruments A and B can be computed. In this case, instrument C provides a transfer function between instruments B and A, whereby c_n can be expressed as the sum of three biases, namely,

$$c_n = E_{\mathrm{A-C}} + E_{\mathrm{C-B}} + E_W \tag{6}$$

where

$$E_{\mathrm{A-C}} \equiv \langle T^{\mathrm{A}} \rangle - \langle T^{\mathrm{AC}} \rangle \tag{7}$$

$$E_{\mathrm{C-B}} \equiv \sum_m \beta_m \left[\langle T_m^{\mathrm{BC}} \rangle - \langle T_m^{\mathrm{B}} \rangle \right] \tag{8}$$

$$E_W \equiv \langle T^{\mathrm{AC}} \rangle - \sum_m \beta_m \langle T_m^{\mathrm{BC}} \rangle \tag{9}$$

where the angled brackets denote a time average, and, as before, all temperatures are deseasonalized. For clarity, we have omitted the subscript n since it is common to all terms. The quantities T^{AC} and T^{BC} denote the temperatures of instrument C that have been averaged in the vertical using the weighting functions for instruments A and B, respectively. The first term ($E_{\mathrm{A-C}}$) in Eq. (6) denotes the relative bias between the temperature of instrument A and the instrument A-weighted temperature of instrument C.

ACPD
15, 10085–10122, 2015

The second term ($E_{\text{C-B}}$) is the same but for instrument B (with a minus sign), where the summation over m is required since we are computing the temperature bias for Channel n of instrument A. The third term (E_W) is the weighting function bias, which accounts for the error in the fits to the weighting functions; this term must be evaluated using the height-dependent temperatures from instrument C. If the period over which the time averages of the different terms in Eq. (6) are computed is the same, then

$$c_n = \langle T^{\text{A}} \rangle + \sum_{m=m_1}^{m_2} \beta_m \langle T_m^{\text{B}} \rangle, \tag{10}$$

in which case instrument C is not needed. The advantage of Eq. (6) over Eq. (10), however, lies in the fact that instrument C enables us to separate the relative biases into different components. Moreover, if there is a gap in time between instruments A and B, but instrument C still overlaps with instruments A and B, then Eq. (10) could not be used.

3.1.3 Merging SSU and AMSU using MIPAS

Here we consider only the case where we extend SSU forward in time, which means that A = SSU and B = AMSU in Eq. (4). While it is certainly possible to extend AMSU backward (i.e., A = AMSU and B = SSU), we do not do so because the weighting function bias terms (E_W) are substantially larger when fitting the three broad SSU weighting functions to the six narrower AMSU weighting functions.

Table 2 shows the different bias terms given in Eq. (6), which are used to compute c_n in Eq. (4). The bottom row lists the sum of the three biases, which are the c_n's. The magnitudes of the individual bias terms are all less than ~ 1 K, with some cancellation between the different terms. The $E_{\text{SSU-MIPAS}}$ term is identical to the offsets between SSU and SSU-weighted MIPAS shown in Fig. 2. The weighting function term E_W is largest for Channel 3 since the fit is the poorest (see Fig. 1). Figure 5 shows the difference between the deseasonalized SSU temperatures and the fitted temperatures computed using AMSU as a function of time, and indicates that the relative biases (whose means are the c_n's) are fairly stable in time. The standard deviations of the differences, which provide a conservative measure of the uncertainty of the fits, are 0.06, 0.09 and 0.09 K for Channels 1, 2 and 3, respectively. These values are clearly much smaller than the dynamic range seen in Fig. 6, which shows the SSU data (black) and the corresponding extension derived from AMSU and MIPAS using Eqs. (4) and (6) for the 1979–2012 time period. Thus, uncertainties in the c_n's have a negligible impact on the temporal behavior of the merged data records. The insets show blow-ups of the two time series in the overlap period, along with the corresponding correlation coefficients r. The agreement between the two time series is very good, with the highest correlation occurring for the lowest channel.

The SSU and fitted SSU deseasonalized temperature time series can be combined into a single time series, which we shall refer to as the extended SSU time series $\widetilde{T}_n^{\mathrm{SSU}}$ (denoted with a tilde), as follows

$$\widetilde{T}_n^{\mathrm{SSU}} = \alpha(t) T_n^{\mathrm{SSU}} + \beta(t) \hat{T}_n^{\mathrm{SSU}} \tag{11}$$

where $\hat{T}_n^{\mathrm{SSU}}$ is the time series computed using Eqs. (4) and (6), and the time-dependent coefficients α and β are given by

$$\begin{aligned} \alpha(t) &= 1 \quad \text{for } t \leq t_1 \\ \alpha(t) &= 1 - \frac{(t - t_1)}{(t_2 - t_1)} \quad \text{for } t_1 \leq t \leq t_2 \\ \alpha(t) &= 0 \quad \text{for } t \geq t_2 \end{aligned}$$

and $\beta = 1 - \alpha$ where $t_1 = 2001.00$ and $t_2 = 2006.25$ are the start and end dates of the overlap period between SSU and AMSU Channel 14. The extended SSU temperatures, expressed as anomalies with respect to the 1980–1985 mean, are shown in Fig. 7 (black curves). The other curves in this figure will be discussed in the next section.

Discussion Paper | Discussion Paper | Discussion Paper | Discussion Paper |

ACPD

15, 10085–10122, 2015

Merging nadir-sounding climate records

C. McLandress et al.

3.2 Stratospheric temperature trends

In this section we take a closer look at the temperature trends in the first decade of this century using not only the AMSU and MIPAS data, but also MLS. We then take a step back and re-examine the long-term trends in the context of model simulations, and reanalyses.

Figure 8 compares AMSU temperatures (black) to the AMSU-weighted results computed from MIPAS (blue) and MLS (red), with the latter two being offset with respect to AMSU for display purposes. The offsets are computed so that the time means in the overlap period are identical to those of AMSU. As remarked earlier, the AMSU-weighted MIPAS temperatures exhibit stronger cooling in the upper channels than do AMSU. MIPAS is known to have a drift due to time-dependent detector-nonlinearity, which had not been considered for the calibration of radiance spectra used here (e.g., Eckert et al., 2014). A latitude and altitude dependent drift of MIPAS temperatures relative to MLS of the order of $-1\,\mathrm{K\,decade^{-1}}$ has been identified for most parts of the stratosphere (Eckert, 2012), which is in agreement with the trend differences found here. A refined calibration, which takes the time-dependence of the detector-nonlinearity into account, is currently under investigation. The MLS results, however, do not show such an effect, and are in fact in better agreement with AMSU on a year-to-year basis.

The temperature trends from MIPAS and MLS computed from 2004–2012 are shown in Fig. 9 as a function of height. Two types of uncertainties are shown. The first assumes the data points are independent (thick error bars and dark shading); this is appropriate when comparing trends between different data sets over the same time period, where the differences will be mainly instrumental. The second takes into account serial correlation using the lag-1 autocorrelation coefficient to estimate the reduced number of degrees of freedom following Santer et al. (2000) (thin error bars and light shading). Since serial correlation is a property of the atmosphere, not of a particular instrument, the lag-1 autocorrelation coefficient computed from the MLS data is used in calculating the reduced number of degrees of freedom for the sparser MIPAS data. Although the time period is relatively short, global-mean temperature exhibits limited internal variability (since it is under radiative control) and so the uncertainties in the trends in the upper stratosphere are relatively low. Superimposed on Fig. 9 are the AMSU trends (black circles) and the AMSU-weighted MLS and MIPAS trends (black squares). The weighted trends lie along the (tilted) axes of the profile trends, since they are a vertically smoothed version of the latter. As was seen in Fig. 8, the agreement between MLS and AMSU is excellent (left panel), while MIPAS shows substantially stronger cooling trends in the upper stratosphere (right panel). The same conclusions can be inferred from the trends from extended SSU (red circles) and SSU-weighted MLS and MIPAS (red squares), computed for the 2004–2012 period, which are also shown on Fig. 9.

Although MLS uses as its a priori an analysis that has assimilated AMSU radiances, the impact of AMSU on the MLS temperatures is thought to be relatively small since the MLS retrievals are more susceptible to vertical variations much shorter than the widths of the AMSU weighting functions (M. Schwartz, personal communication, 2014). We therefore believe that the good agreement between MLS and AMSU is real and therefore an independent validation of the MLS data, while the strong cooling in the MIPAS data is attributed to its known drift. It is not clear whether the strong vertical structure seen in the MLS profile trends is real, given the similarity of the extended SSU and the AMSU trends.

We now return to Fig. 7, which shows the extended SSU temperature anomalies (with respect to 1980–1985) plotted from 1979 to 2012, with the intent of shedding light on the mismatch between SSU and models highlighted in Thompson et al. (2012). As in their study, we compare our results to the CCMVal2 models. Near-global mean temperatures are constructed from monthly means and vertically averaged using the SSU weighting functions using Eq. (1), with the limits of integrations being $z_b = 0$ km and $z_t =$ the height corresponding to the top pressure level provided by each model data file. In contrast to the findings of Thompson et al. (2012), the results shown in

Discussion Paper | Discussion Paper | Discussion Paper | Discussion Paper |

ACPD
15, 10085–10122, 2015

Merging nadir-sounding climate records

C. McLandress et al.

Fig. 7 indicate good qualitative agreement between extended SSU (black) and the CCMVal2 multi-model mean (red) for all three SSU channels. The differences between our results and those of Thompson et al. have arisen because they were using version 1 of the NOAA SSU data.

Since the CCMVal2 simulations ended about the same year as the SSU measurements, they cannot be used to compare to the extended SSU data post 2006. However, Thompson et al. (2012) also showed results for the climate-model simulations from the Coupled Model Intercomparison Project Phase 5 (CMIP5) (their Fig. 1), which do extend beyond 2006. Comparing our extended SSU results to the CMIP5 results in Thompson et al. indicates good qualitative agreement, with both data sets exhibiting continued stratospheric cooling after 2006 followed by warming starting in about 2009. The cooling is due to a combination of the effects of increasing CO_2 and the declining phase of the previous solar cycle, while the warming is presumably due to the current solar cycle which commenced in 2008. Since the SSU-weighted CCMVal2 and CMIP5 results track each other reasonably well prior to 2006, this suggests overall consistency between the extended SSU record over 1979–2011 and chemistry-climate models.

The blue curves shown in Fig. 7 are the SSU-weighted ERA-Interim temperatures, which have been computed with the addition of the CMAM30 data to fill above 1 hPa (the top level of ERA-Interim) before evaluating the weighting integral given by Eq. (1). Overall they follow the ups and downs of the extended SSU data, but exhibit several jumps, e.g., 1985 and 1998, when new satellite data are assimilated. There is good agreement (with the exception of the offsets) between extended SSU and ERA-Interim after 2006. Since this is the time period when only AMSU data are used to construct the extended SSU record, this good agreement is further validation of our merging approach. The green curves in Fig. 7 are for the adjusted ERA-Interim temperatures, in which the upper stratosphere temperature jumps in 1985 and 1998 have been removed, as described in McLandress et al. (2014). The adjusted time series more closely match the extended SSU results after 1992, but not so from 1985 to

1992, suggesting that the temperature discontinuity in 1985 cannot be simply removed by a constant offset as was done in McLandress et al. (2014).

Figure 10 quantifies near-global mean temperature differences computed for three time periods for SSU (red circles) and the CCMVal2 models (black squares and curves). We prefer differences to linear trends for this purpose because of the non-linear nature of the long-term changes. The left panel shows the differences over the 1981–2004 period. We choose this period to allow a two-year averaging period around each end point. Both observations and models show increasing cooling (negative differences) with altitude; for SSU, this varies from about -1.5 ± 0.1 K (standard deviation, a conservative measure of uncertainty) for Channel 1 to $\sim -2.2 \pm 0.2$ K for Channel 3. These values are consistent with the linear trend values quoted by Zou et al. (2014) for the Version 2 SSU data over the 1979–2006 period, which range from -0.69 ± 0.18 K decade^{-1} (95 % confidence) for Channel 1 to -0.85 ± 0.15 K decade^{-1} for Channel 3. Although the SSU difference for Channel 3 is considerably weaker than the model temperature difference profiles (black curves) at the altitudes where the weighting function peaks, the SSU-simulated model difference for Channel 3 is entirely consistent with the SSU difference. This emphasizes again the point made above that nadir measurements should never be directly compared with profile measurements. The weighted model differences are similarly consistent with SSU for Channel 2, but are somewhat weaker for Channel 1. The latter is consistent with the known underestimation of long-term lower stratospheric cooling in chemistry-climate models, as seen in the comparison with MSU Channel 4 (Thompson et al., 2012) whose long-term trend is considered highly reliable. The reasons for the model underestimation of lower-stratospheric cooling are not known; see Chapter 4 of WMO (2014) for a discussion.

The middle and right panels of Fig. 10 compare the two recent decadal periods between solar minima, to minimize the impact of solar variability which clearly has a large modulating effect on the long-term cooling. For SSU, distinct cooling of about -0.7 K is seen at all levels over 1986–1995, which is a period of strong ozone depletion, whereas negligible cooling is found over 1995–2004 which corresponds to the start of ozone recovery. This highlights the important role of ozone depletion in the observed stratospheric cooling up to the mid-1990 s. A similar though somewhat less pronounced contrast between the two periods is seen in the temperature differences from the models.

4 Conclusions

We present a physically based method for merging near-global mean brightness temperatures from SSU and AMSU using measurements from a third instrument, in this case MIPAS, which has high enough vertical resolution that it can sufficiently accurately simulate the vertically weighted temperatures of both SSU and AMSU. The SSU temperatures are expressed as a linear combination of AMSU temperatures, with the coefficients determined by fitting the AMSU weighting functions to the SSU weighting functions. The MIPAS data is used in matching the SSU temperatures and the AMSU-simulated SSU temperatures.

Multiple linear regression does not work for merging the SSU and AMSU temperatures because the AMSU channels are not sufficiently linearly independent (in a statistical sense) and thus the determination of the regression coefficients is underconstrained. Part of the correlation between the channels arises from the overlap of the weighting functions, but part is also geophysical.

The relative bias between SSU and the AMSU-simulated SSU channels is expressed as a sum of three relative biases: between SSU and MIPAS, between the SSU channels and the AMSU-simulated SSU channels (both applied to MIPAS data), and between MIPAS and AMSU. In this way, MIPAS is used as a transfer function between SSU and AMSU.

In this particular case, SSU and AMSU overlap in time and so a transfer function is not strictly required, but our method would be applicable in cases where the two data sets to be merged did not overlap in time, so long as there was a higher resolution data set that bridged between them. Also, this method allows for quantification of the error

ACPD
15, 10085–10122, 2015

incurred by the approximation of the SSU weighting functions by the AMSU weighting functions.

MIPAS was found to track the three SSU channels and the six AMSU channels very well in time, in both their seasonal cycle and their interannual variability. This provides well-defined relative biases between MIPAS and the two nadir instruments, allowing for the merging of the two nadir records to be performed with confidence. In particular, the standard deviation of the differences during the overlap period is less than 0.1 K for all three SSU channels, which is much less than the dynamic range of the time series. Thus, uncertainties in the merging make a negligible contribution to the long-term changes. The relative bias that results from imperfect approximation of the SSU weighting functions by the AMSU weighting functions is a significant contributor to the overall relative bias for SSU channels 1 and 2, and the dominant contributor for channel 3.

Because global-mean temperature exhibits relatively little interannual variability, compared to the temperature in particular latitude bands, trends can be determined with confidence even over relatively short records. We analyze trends over the period 2004–2012 when data from a second vertically resolved temperature data set, Aura MLS, is available. While MLS temperature trends are essentially identical to those of AMSU, the current version of MIPAS data shows a cooling trend relative to AMSU, which is in agreement with preceding drift analyses (Eckert, 2012). This does not compromise the use of MIPAS as a transfer function between SSU and AMSU, because the relative biases are computed for a particular period, nor for the use of MIPAS data to examine seasonal cycles and interannual variability. However, this version of MIPAS temperature should not be used to determine long-term trends. On the other hand, the high level of agreement between MLS and AMSU provides confidence in both data sets for trend analysis. Over the 2004–2012 period these data show a statistically significant cooling ranging from $\sim 0.6 \pm 0.3\,\mathrm{K\,decade}^{-1}$ for Channel 14 to $\sim 0.3 \pm 0.2\,\mathrm{K\,decade}^{-1}$ for Channel 12, and no statistically significant change for the three lowest Channels 9, 10 and 11.

ACPD
15, 10085–10122, 2015

Merging nadir-sounding climate records

C. McLandress et al.

It is worth noting that even the narrower weighting functions that characterize the AMSU channels, relative to the deeper weighting functions of the SSU channels, strongly smooth the vertical structure seen in the MLS trends. Thus, nadir measurements should never be compared with profile trends derived from higher vertical resolution instruments or models; the latter must always be first filtered through the weighting functions of the nadir measurements.

The long-term stratospheric near global-mean temperature record since 1979, which is represented by the SSU channels, exhibits considerable temporal structure associated with cooling from increasing CO_2 and from ODS-induced ozone depletion, the effects of the solar cycle, and warming from volcanic eruptions. Version 2 of the NOAA SSU record is consistent with the behaviour seen in chemistry-climate model simulations. This is in contrast to the findings of Thompson et al. (2012) who examined Version 1 of that data. In particular, both the SSU record and the models show the same contrast between cooling trends between recent solar minima (so as to minimize the effects of solar variability), with weak cooling over 1995–2004 compared with the large cooling seen in the period 1986–1995 of strong ozone depletion. The AMSU-simulated SSU channels show a continued cooling beyond the end of the SSU record, although there is a small warming in the last few years (up to 2011) which is presumably associated with the solar cycle. Thus, the extended SSU global-mean temperature record constructed here, which covers 1979–2011, is consistent with physical expectations of the vertical structure and temporal variations in the rates of stratospheric cooling over this period.

Acknowledgements. Funding for Charles McLandress and Andreas Jonsson was provided from the European Space Agency. The authors thank Gloria Manney for providing the Aura MLS data and also for helpful discussions. Charles McLandress thanks David Plummer for providing some diagnostic code.

ACPD
15, 10085–10122, 2015

References

Dee, D. P., Uppala, S. M., Simmons, A. J., Berrisford, P., Poli, P., Kobayashi, S., Andrae, U., Balmaseda, M. A., Balsamo, G., Bauer, P., Bechtold, P., Beljaars, A. C. M., van de Berg, L., Bidlot, J., Bormann, N., Delsol, C., Dragani, R., Fuentes, M., Geer, A. J., Haimberger, L., Healy, S. B., Hersbach, H., Hólm, E. V., Isaksen, L., Kållberg, P., Köhler, M., Matricardi, M., McNally, A. P., Monge-Sanz, B. M., Morcrette, J.-J., Park, B.-K., Peubey, C., de Rosnay, P., Tavolato, C., Thépaut, J. N., and Vitart, F.: The ERA-Interim reanalysis: configuration and performance of the data assimilation system, Q. J. Roy. Meteor. Soc., 137, 553–597, doi:10.1002/qj.828, 2011.

Eckert, E.: Drifts and Trends in MIPAS Temperature and Ozone Measurements, Ph.D. thesis, Karlsruhe Institute of Technology, 2012.

Eckert, E., von Clarmann, T., Kiefer, M., Stiller, G. P., Lossow, S., Glatthor, N., Degenstein, D. A., Froidevaux, L., Godin-Beekmann, S., Leblanc, T., McDermid, S., Pastel, M., Steinbrecht, W., Swart, D. P. J., Walker, K. A., and Bernath, P. F.: Drift-corrected trends and periodic variations in MIPAS IMK/IAA ozone measurements, Atmos. Chem. Phys., 14, 2571–2589, doi:10.5194/acp-14-2571-2014, 2014.

Fischer, H., Birk, M., Blom, C., Carli, B., Carlotti, M., von Clarmann, T., Delbouille, L., Dudhia, A., Ehhalt, D., Endemann, M., Flaud, J. M., Gessner, R., Kleinert, A., Koopman, R., Langen, J., López-Puertas, M., Mosner, P., Nett, H., Oelhaf, H., Perron, G., Remedios, J., Ridolfi, M., Stiller, G., and Zander, R.: MIPAS: an instrument for atmospheric and climate research, Atmos. Chem. Phys., 8, 2151–2188, doi:10.5194/acp-8-2151-2008, 2008.

Fomichev, V. I.: The radiative energy budget of the middle atmosphere and its parameterization in general circulation models, J. Atmos. Sol.-Terr. Phys., 71, 1577–1585, 2009.

Hegglin, M. I., Tegtmeier, S., Anderson, J., Froidevaux, L., Fuller, R., Funke, B., Jones, A., Lingenfelser, G., Lumpe, J., Pendlebury, D., Remsberg, E., Rozanov, A., Toohey, M., Urban, J., von Clarmann, T., Walker, K. A., Wang, R., and Weigel, K.: SPARC Data Initiative: comparison of water vapor climatologies from international satellite limb sounders, J. Geophys. Res., 118, 11824–11846, doi:10.1002/jgrd.50752, 2013.

Hegglin, M. I., Plummer, D. A., Shepherd, T. G., Scinocca, J. F., Anderson, J., Froidevaux, L., Funke, B., Hurst, D., Rozanov, A., Urban, J., von Clarmann, T., Walker, K. A., Wang, H. J., Tegtmeier, S., and Weigel, K.: Vertical structure of stratospheric water vapour trends derived from merged satellite data, Nat. Geosci., 7, 768–776, 2014.

ACPD
15, 10085–10122, 2015

Intergovernmental Panel on Climate Change (IPCC): Climate Change 2013: the physical scientific basis, edited by: Stocker, T. F., Qin, D., Plattner, G.-K., Tignor, M., Allen, S. K., Boschung, J., Nauels, A., Xia, Y., Bex, V., and Midgley, P. M., Cambridge University Press, New York, 1535 pp., 2013.

Livesey, N. J., Read, W. G., Froideveaux, L., Lambert, A., Manney, G. L., Pumphrey, H. C., Santee, M. L., Schwartz, M. J., Wang, S., Cofield, R. E., Cuddy, D. T., Fuller, R. A., Jarnot, R. F., Jiang, J. H., Knosp, B. W., Stek, P. C., Wagner, P. A., and Wu, D. L.: Version 3.3 Level 2 data quality and description document. Tech. Rep. JPL D-33509, Jet Propulsion Laboratory, available at: https://mls.jpl.nasa.gov/data/datadocs.php (last access: 30 March 2015), 2011.

McLandress, C., Plummer, D. A., and Shepherd, T. G.: Technical Note: A simple procedure for removing temporal discontinuities in ERA-Interim upper stratospheric temperatures for use in nudged chemistry-climate model simulations, Atmos. Chem. Phys., 14, 1547–1555, doi:10.5194/acp-14-1547-2014, 2014.

Randel, W. J., Shine, K. P., Austin, J., Barnett, J., Claud, C., Gillett, N. P., Keckhut, P., Langematz, U., Lin, R., Long, C., Mears, C., Miller, A., Nash, J., Seidel, D. J., Thompson, D. W. J., Wu, F., and Yoden, S.: An update of observed stratospheric temperature trends, J. Geophys. Res., 114, D02107, doi:10.1029/2008JD010421, 2009.

Santer, B. D., Wigley, T. M. L., Boyle, J. S., Gaffen, J. S., Hnilo, J. J., Nychka, D., Parker, D. E., and Taylor, K. E.: Statistical significance of trends and trend differences in layer-average atmospheric time series, J. Geophys. Res., 105, 7337–7356, 2000.

Schwartz, M. J., Lambert, A., Manney, G. L., Read, W. G., Livesay, N. J., Froideveaux, L., Ao, C. O., Bernath, P. F., Boone, C. D., Cofield, R. E., Daffer, W. H., Drouin, B. J., Fetzer, E. J., Fuller, R. A., Jarnot, R. F., Jiang, J. H., Jiang, Y. B., Knosp, B. W., Krüger, K., Li, J.-L. F., Mlynczak, M. G., Pawson, S., Russell, J. M. III, Santee, M. L., Synder, W. V., Stek, P. C., Thurstans, R. P., Tompkins, A. M., Wagner, P. A., Walker, K. A., Waters, J. W., and Wu, D. L.: Validation of the Aura Microwave Limb Sounder temperature and geopotential height measurements, J. Geophys. Res., 113, D15S11, doi:10.1029/2007JD008783, 2008.

Shepherd, T. G. and Jonsson, A. I.: On the attribution of stratospheric ozone and temperature changes to changes in ozone-depleting substances and well-mixed greenhouse gases, Atmos. Chem. Phys., 8, 1435–1444, doi:10.5194/acp-8-1435-2008, 2008.

Shine, K. P., Bourqui, M. S., de Forster, P. M., Hare, S. H. E., Langematz, U., Braesicke, P., Grewe, V., Ponater, M., Schnadt, C., Smith, C. A., Haigh, J. D., Austin, J., Butchart, N., Shindell, D. T., Randel, W. J., Nagashima, T., Portmann, R. W., Solomon, S., Seidel, D. J.,

ACPD

15, 10085–10122, 2015

Lanzante, J., Klein, S., Ramaswamy, V., and Schwartzkopf, M. D.,: A comparison of model-simulated trends in stratospheric temperatures, Q. J. Roy. Meteor. Soc., 129, 1565–1588, doi:10.1256/qj.02.186, 2003.

Solomon, S., Rosenlof, K. H., Portmann, R. W., Daniel, J. S., Davis, S. M., Sanford, T. J., and Plattner, G.-K.: Contributions of stratospheric water vapor changes to decadal variation in the rate of global warming, Science, 327, 1219–1222, 2010.

Stiller, G. P., Kiefer, M., Eckert, E., von Clarmann, T., Kellmann, S., García-Comas, M., Funke, B., Leblanc, T., Fetzer, E., Froidevaux, L., Gomez, M., Hall, E., Hurst, D., Jordan, A., Kämpfer, N., Lambert, A., McDermid, I. S., McGee, T., Miloshevich, L., Nedoluha, G., Read, W., Schneider, M., Schwartz, M., Straub, C., Toon, G., Twigg, L. W., Walker, K., and Whiteman, D. N.: Validation of MIPAS IMK/IAA temperature, water vapor, and ozone profiles with MOHAVE-2009 campaign measurements, Atmos. Meas. Tech., 5, 289–320, doi:10.5194/amt-5-289-2012, 2012.

Thompson, D. W. J., Seidel, D. J., Randel, W. J., Zou, C.-Z., Butler, A. H., Mears, C., Osso, A., Long, C., and Lin, R.: The mystery of recent stratospheric temperature trends, Nature, 491, 692–697, doi:10.1038/nature11579, 2012.

von Clarmann, T., Glatthor, N., Grabowski, U., Höpfner, M., Kellmann, S., Kiefer, M., Linden, A., Mengistu Tsidu, G., Milz, M., Steck, T., Stiller, G. P., Wang, D. Y., Fischer, H., Funke, B., Gil-López, S., and López-Puertas, M.: Retrieval of temperature and tangent altitude pointing from limb emission spectra recorded from space by the Michelson Interferometer for Passive Atmospheric Sounding (MIPAS), J. Geophys. Res., 108, D23, doi:10.1029/2003JD003602, 2003.

von Clarmann, T., Höpfner, M., Kellmann, S., Linden, A., Chauhan, S., Funke, B., Grabowski, U., Glatthor, N., Kiefer, M., Schieferdecker, T., Stiller, G. P., and Versick, S.: Retrieval of temperature, H_2O, O_3, HNO_3, CH_4, N_2O, $ClONO_2$ and ClO from MIPAS reduced resolution nominal mode limb emission measurements, Atmos. Meas. Tech., 2, 159–175, doi:10.5194/amt-2-159-2009, 2009.

Wang, D. Y., von Clarmann, T., Fischer, H., Funke, B., Gil-López, S., Glatthor, N., Grabowski, U., Höpfner, M., Kaufmann, M., Kellmann, S., Kiefer, M., Koukouli, M. E., Linden, A., López-Puertas, M., Mengistu Tsidu, G., Milz, M., Steck, T., Stiller, G. P., Simmons, A. J., Dethof, A., Swinbank, R., Marquardt, C., Jiang, J. H., Romans, L. J., Wickert, J., Schmidt, T., Russell III, J., and Remsberg, E.,: Validation of stratospheric temperatures measured by Michelson

ACPD
15, 10085–10122, 2015

Merging nadir-sounding climate records

C. McLandress et al.

Interferometer for Passive Atmospheric Sounding (MIPAS) on Envisat, J. Geophys. Res., 110, D08301, doi:10.1029/2004JD005342, 2005.

Wang, L. and Zou, C.-Z.: AMSU-A-Only atmospheric temperature data records from the lower troposphere to the top of the stratosphere, J. Atmos. Ocean. Tech., 31, 808–825, doi:10.1175/JTECH-D-13-00134.1, 2014.

Wang, L., Zou, C.-Z., and Qian, H.: Construction of stratospheric temperature data records from Stratospheric Sounding Units, J. Climate, 25, 2931–2946, doi:10.1175/JCLI-D-11-00350.1, 2012.

World Meteorological Organization (WMO): Scientific Assessment of Ozone Depletion: 2014, World Meteorological Organization, Global Ozone Research and Monitoring Project – Report No. 55, 416 pp., Geneva, Switzerland, 2014.

Zou, C.-Z., Qian, H., Wang, W., Wang, L., and Long, C.,: Recalibration and merging of SSU observations for stratospheric temperature trend studies, J. Geophys. Res., 119, 13180–13205, doi:10.1002/2014JD021603, 2014.

ACPD
15, 10085–10122, 2015

Table 1. Unnormalized coefficients β_m for AMSU Channels $m = 9$–14 of the fits to the three SSU weighting functions $n = 1$–3 used in Eq. (3).

AMSU channel (m)	SSU ($n = 1$)	SSU ($n = 2$)	SSU ($n = 3$)
14	0.018	0.313	0.786
13	0.114	0.300	−0.267
12	0.422	0.185	0.334
11	0.226	0.100	−0.117
10	0.146	0.048	0.098
9	0.053	0.021	−0.017

ACPD
15, 10085–10122, 2015

Merging nadir-sounding climate records

C. McLandress et al.

ACPD
15, 10085–10122, 2015

Merging nadir-sounding climate records

C. McLandress et al.

Table 2. The three bias terms in the expression for c_n in Eq. (6) for $n = 1$–3 in the case where instrument A = SSU, B = AMSU and C = MIPAS. Units are K. The sum of the terms, which is listed in the bottom row, is the constant c_n used in Eq. (4). See text for details.

Bias	SSU ($n = 1$)	SSU ($n = 2$)	SSU ($n = 3$)
$E_{\text{SSU-MIPAS}}$	−0.173	−0.744	−0.241
$E_{\text{MIPAS-AMSU}}$	0.087	0.007	−0.686
E_W	0.398	0.334	1.196
Sum (c_n)	0.312	−0.403	0.269

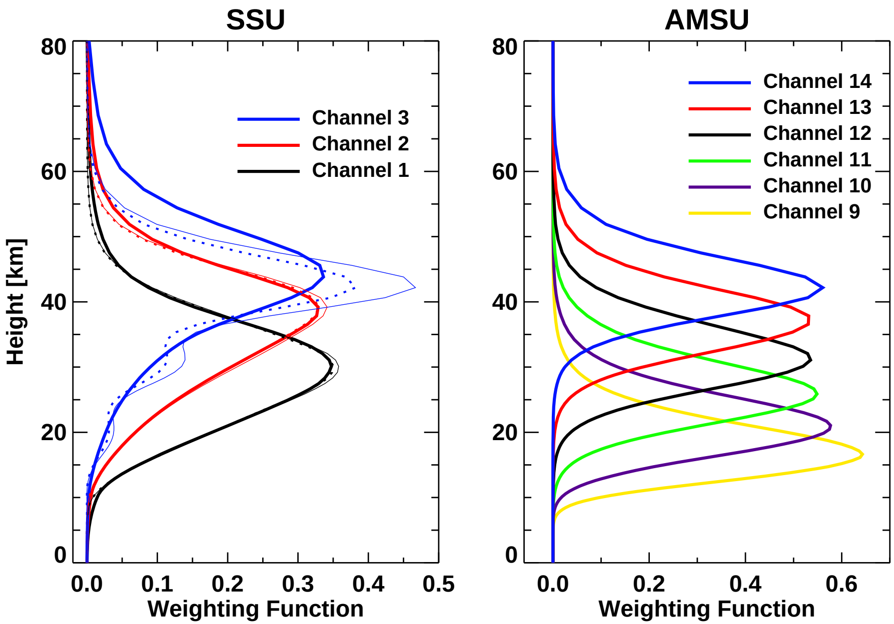

Figure 1. Vertical weighting functions (thick solid curves) for SSU (left) and AMSU (right). The thin solid and dotted curves in the left panel are, respectively, the normalized and unnormalized fits to the SSU weighting functions obtained using the AMSU weighting functions using Eq. (3); see text for details.

ACPD
15, 10085–10122, 2015

Merging nadir-sounding climate records

C. McLandress et al.

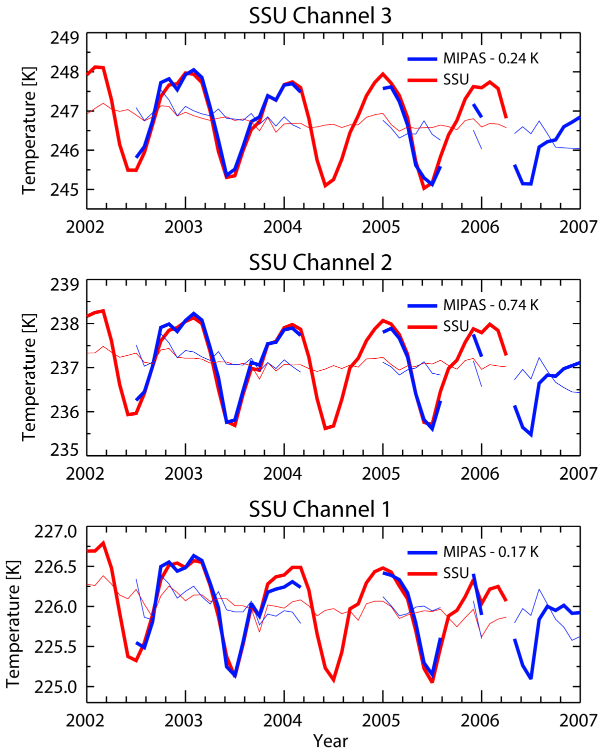

Figure 2. SSU (red) and SSU-weighted MIPAS (blue) temperatures for Channels 1–3. The thin curves are the deseasonalized temperatures. The weighted MIPAS temperatures are offset by a constant amount so that the mean difference between the deseasonalized SSU and MIPAS time series is zero; the value of this offset is labeled in each panel. In this and all other figures, monthly and near-global (75° S–75° N) means are shown, and the tick marks directly above each year label on the horizontal axes are for January of that year.

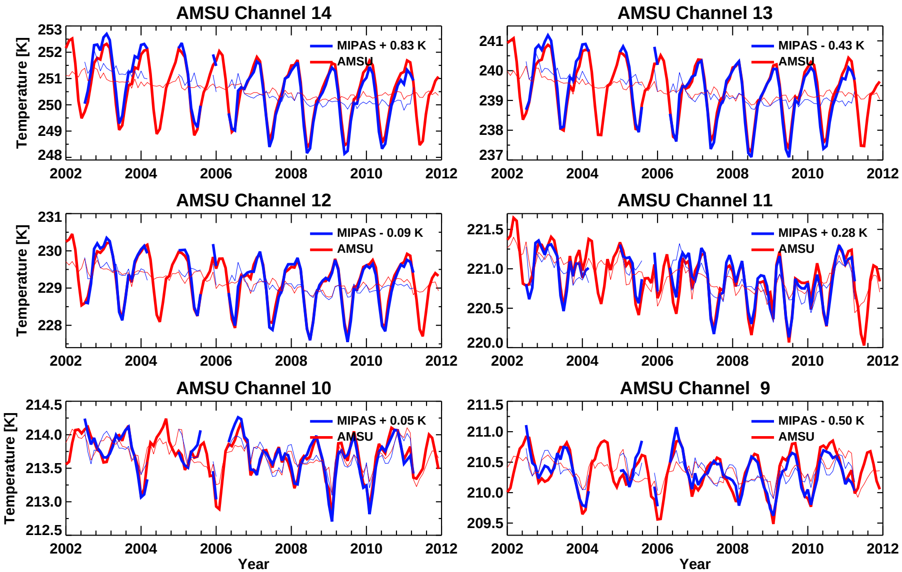

Figure 3. AMSU (red) and AMSU-weighted MIPAS (blue) temperatures for Channels 9–14. The thin curves denote the deseasonalized temperatures. See the Fig. 2 caption for more details.

ACPD
15, 10085–10122, 2015

Merging nadir-sounding climate records

C. McLandress et al.

Title Page
Abstract | Introduction
Conclusions | References
Tables | Figures
◀| |▶
◀ ▶
Back | Close
Full Screen / Esc
Printer-friendly Version
Interactive Discussion

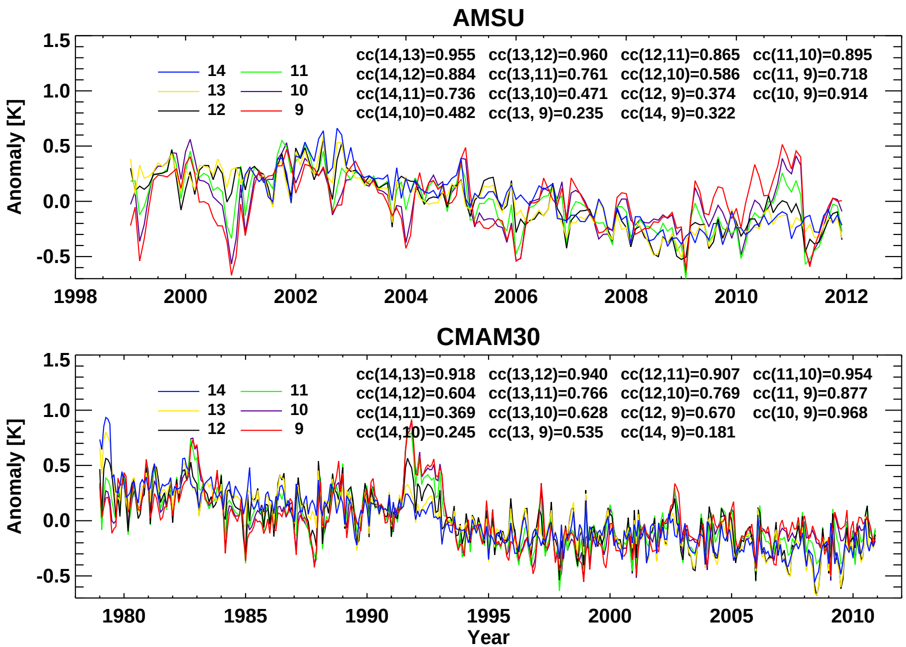

Figure 4. Top: deseasonalized AMSU temperature anomalies with respect to the 1999–2011 mean for Channels 9 to 13 and the 2001–2011 mean for Channel 14, with the variance of each channel normalized to 0.25 K^2. Bottom: same but for AMSU-weighted CMAM30 for the 1979 to 2011 time period. The correlation coefficient between the different channels is labeled in each panel.

ACPD
15, 10085–10122, 2015

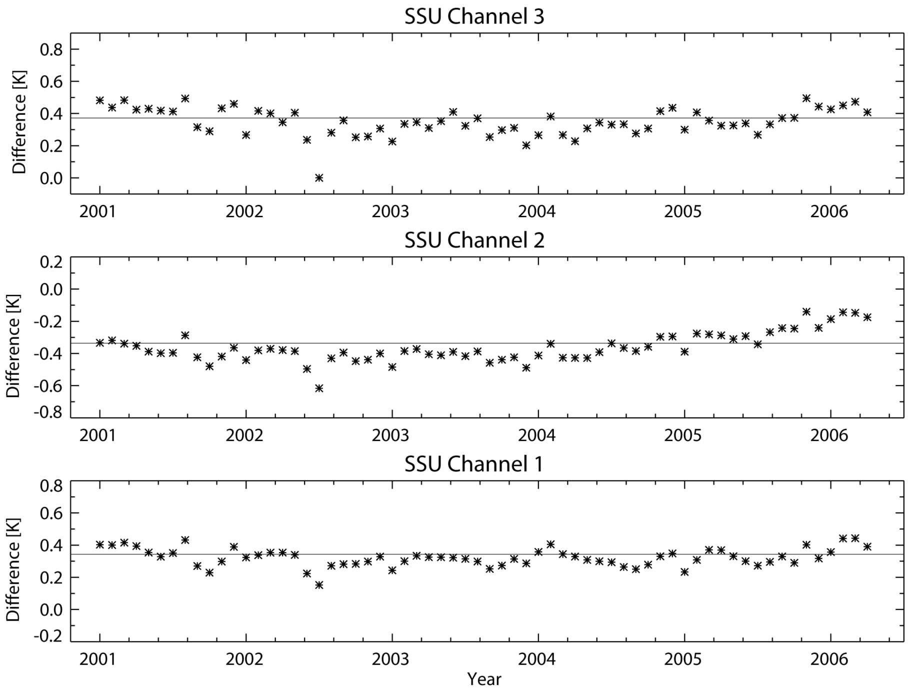

Figure 5. Difference between the deseasonalized SSU temperatures and the fitted temperatures computed using AMSU, i.e., $T_n^{\mathrm{SSU}} - \sum_{m=m_1}^{m_2} \beta_m T_m^{\mathrm{AMSU}}$. The horizontal lines are the constants c_n used in Eq. (4). See text for more details.

ACPD
15, 10085–10122, 2015

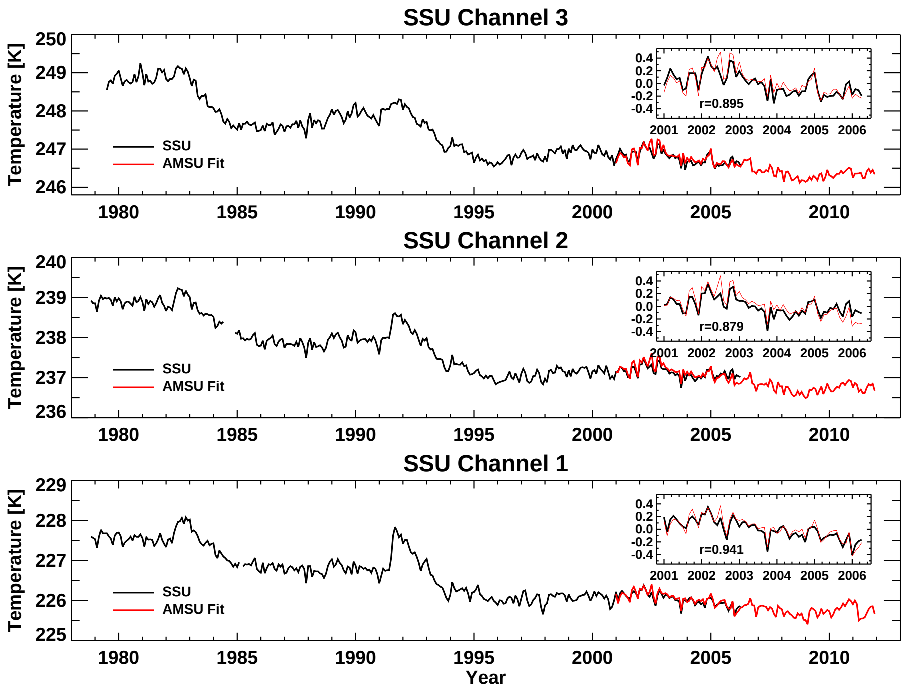

Figure 6. Deseasonalized temperatures for SSU Channels 1–3 (black) and the fits computed from AMSU (red) using Eqs. (4) and (6). The insets show blow-ups of the time series in the overlap period (with the SSU time means subtracted off), along with the correlation coefficients (r) between each pair of curves.

ACPD
15, 10085–10122, 2015

Merging nadir-sounding climate records

C. McLandress et al.

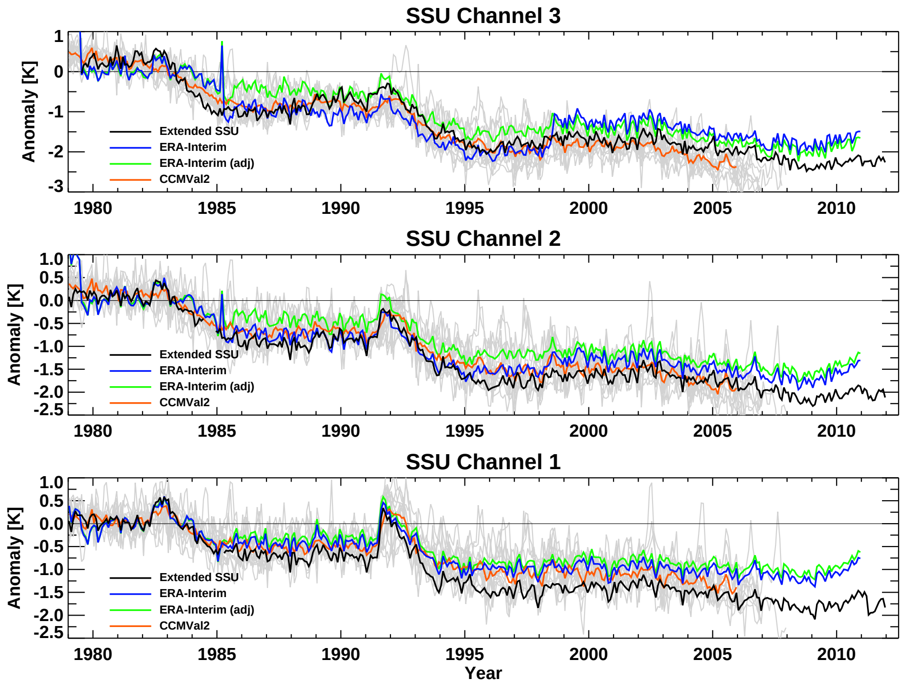

Figure 7. Deseasonalized temperature anomalies for extended SSU (black), ERA-Interim (blue), adjusted ERA-Interim where the jumps in 1985 and 1998 have been removed (green), and the CCMVal2 multi-model mean (red). The light gray curves are the time series of the individual models used to compute the multi-model mean. The anomalies are computed with respect to 1980–1985, such that the time mean anomaly over this period is zero. The extended SSU time series is the one generated using Eq. (4). The slight constant offset (∼ 0.2 K) between ERA-Interim and adjusted ERA-Interim has resulted because the global-mean adjustments have been applied here to the near-global mean temperatures.

ACPD
15, 10085–10122, 2015

Merging nadir-sounding climate records

C. McLandress et al.

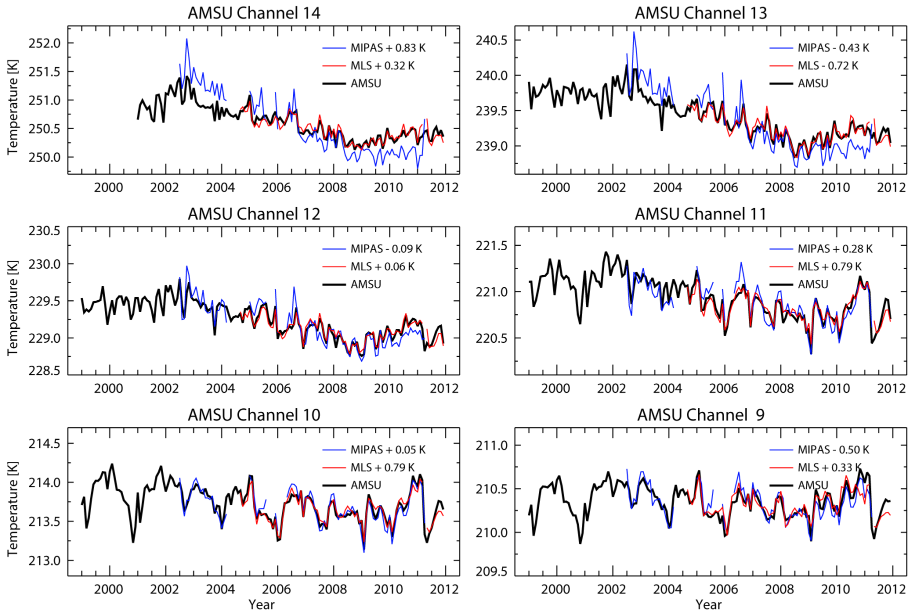

Figure 8. Deseseasonalized temperatures for AMSU Channels 9–14 (black) and the corresponding AMSU-weighted temperatures computed from MIPAS (blue) and MLS (red). The constant offsets between MIPAS and AMSU and between MLS and AMSU are labeled in each panel.

ACPD
15, 10085–10122, 2015

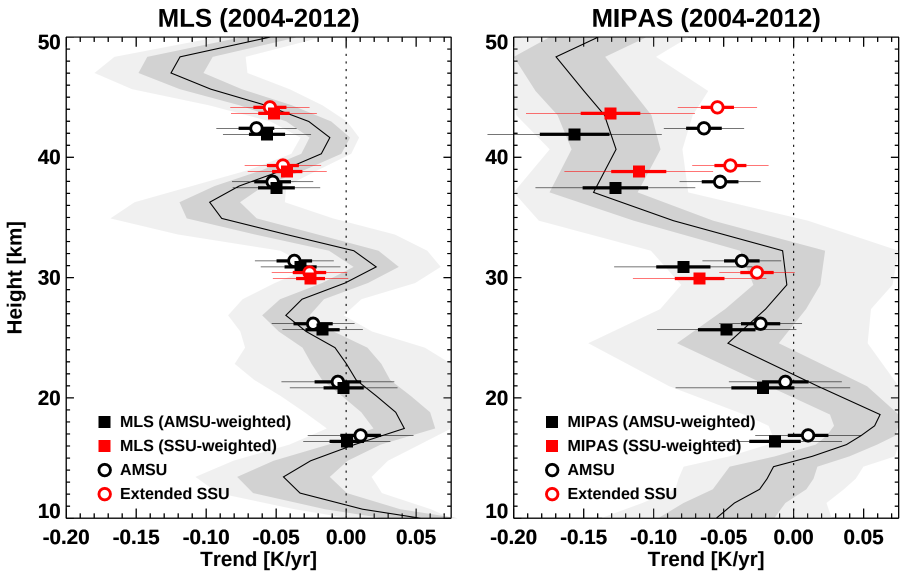

Figure 9. Linear temperature trends for MLS (left) and MIPAS (right) computed from 2004–2012. The solid curves are computed from the height-dependent data; the black and red squares are the corresponding AMSU-weighted and SSU-weighted results plotted at the heights of the weighting function maxima shown in Fig. 1 and offset slightly in the vertical for clarity. The black and red circles are the corresponding trends from AMSU and extended SSU. The Channel numbers range from 14 (3) at the top to 9 (1) at the bottom for AMSU (SSU). The dark and light grey shading, as well as the thick and thin error bars, denote the 95 % confidence levels computed assuming, respectively, independent and serially correlated data; see text for details.

Discussion Paper | Discussion Paper | Discussion Paper | Discussion Paper |

ACPD
15, 10085–10122, 2015

Merging nadir-sounding climate records

C. McLandress et al.

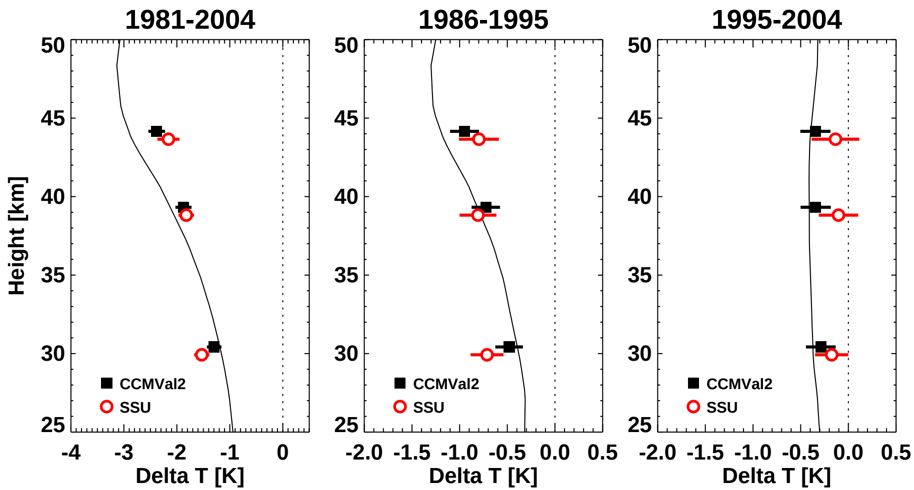

Figure 10. Temperature differences for SSU and the CCMVal2 multi-model mean computed for the following three periods: 1981–2004 (left), 1986–1995 (middle) and 1995–2004 (right). The CCMVal2 temperature difference profiles are given by the black curves, the SSU-weighted CCMVal2 differences by the black squares and the SSU differences by the red circles. The latter two are plotted at the heights of the maxima of the three SSU weighting functions, ranging from Channel 3 at the top to Channel 1 at the bottom; the symbols are offset slightly in the vertical for clarity. The error bars denote plus and minus one standard deviation. The differences are computed from data that have been averaged over two years spanning each of the two end points.